Combined atomistic simulations to explore metastability and substrate effects in Ag-Co nanoalloy systems

Abir Hizi, Georg Daniel Förster, Riccardo Ferrando, Yves Garreau, Alessandro Coati, Caroline Andreazza-Vignolle, Pascal Andreazza

Journal Name

ARTICLE TYPE

Cite this: DOI: 00.0000/xxxxxxxxxx

Combined atomistic simulations to explore metastability and substrate effects in Ag-Co nanoalloy systems†

Abir Hizi,[a] Georg Daniel Forster,*[a] Riccardo Ferrando,[b] Yves Garreau,[c] Alessandro Coati,[d] Caroline Andreazza-Vignolle[a] and Pascal Andreazza*[a]

Received Date
Accepted Date

DOI: 00.0000/xxxxxxxxxx

The Ag/Co nanoalloy system is a model system situated energetically at the limit of stability of the core-shell chemical ordering with respect to a simple phase separation behavior. This makes the system highly susceptible to effects of the environment, such as interaction with a substrate. However, kinetic effects may also be exploited by careful atom-by-atom particle growth that allows to lock in certain out-of-equilibrium configurations, such as off-center, quasi-Janus and even Janus type particles. In this contribution, we explore to what extent out-of-equilibrium structures are due to kinetic effects and the influence of the interaction of the particles with an amorphous carbon substrate by a joint experimental and molecular dynamics study. The simulation set up performed at 300 K and 600 K mimicks the experimental growth process. The substrate deforms the particles, but has also an ordering effect on particle orientation and particle stability. In case of growth of Ag on Co seeds, particles assume close to equilibrium quasi-Janus structure, while for the deposition of Co on Ag seeds, highly out-of-equilbrium structures with several subsurface Co clusters are obtained.

1 Introduction

Multimetallic nanoparticles present properties with a high degree of tunability, which is a consequence of the great variety of atomic arrangements that they can present[1]. The structure of such nanoalloys is specified by its geometric configuration, which can be crystalline or noncrystalline, and by its chemical ordering, which is the pattern in which the two or more metals are arranged within the geometric structure. A bimetallic nanoparticle AB can present various chemical orderings, ranging from a mixed to a completely segregated morphology[2–4]. Mixed alloys can be either random or ordered, as is the case for the $L1_0$ geometry of Co-Pt and Au-Ag alloys[5–7] whereas segregated motifs often manifest themselves as a core-shell order where a core of metal A is surrounded by an external B shell[8,9] or as a bicompartmentalized configuration, where the A and B metals are separated in two domains as Janus particles[2].

When the components of nanoalloys are weakly miscible, especially in the case of Cu-Ag, Ni-Ag, and Co-Ag with high differences in cohesive energy, core-shell and quasi-Janus chemical orderings are expected at equilibrium in wide composition ranges. In core-shell nanoalloys, an external shell of the surface-segregating element (in these cases, Ag is expected) covers a core of the more cohesive element M (M being either Cu, Ni, or Co)[10–14]. In the quasi-Janus structure, the core is in off-center position, so that it is covered by a very thin layer of the shell element on one of its sides[12]. Among these, the AgCo system belongs to the class of materials composed by immiscible ferromagnetic and nonmagnetic elements, a mixture which raises interest as it can exhibit giant magnetoresistance effects[15]. The second interest is the combination of magnetic and plasmonic effects, from Co and Ag respectively[16], not only to increase the frequency variation range of the plasmon resonance, but also to guarantee stability of optical properties of the devices with time.

However, our main motivation is elsewhere, focusing on structure, to determine not only the "expected" core-shell or Janus-like segregated equilibrium structures as a function of size and composition, but also the influence of growth kinetics the interaction with an amorphous carbon substrate. Indeed, the formation of a nanosystem is a process that does not often lead to the equilibrium structure: the system can take different possible metastable structures (free energy minima separated by barriers), each holding the dynamics for a long time compared to the fast vibrations of the bonds, until a jump is finally made to another metastable state. Basically, time is the key to transition phenomena: it characterizes the kinetics of the process in the form of a velocity

[a] Interfaces, Confinement, Matériaux et Nanostructures, ICMN, Université d'Orléans, CNRS, Orléans, France.
[b] Physics Department, University of Genoa, and CNR-IMEM, Genoa, Italy.
[c] MPQ, Université de Paris, CNRS, Paris, France.
[d] Synchrotron Soleil, Gif-sur-Yvette, France.
* Corresponding authors, e-mail georg-daniel.forster@univ-orleans.fr; pascal.andreazza@univ-orleans.fr.
† Electronic Supplementary Information (ESI) available: Experimental results details. See DOI: 00.0000/00000000.

that can be very slow (for example, the nucleation rate). This is a formidable barrier between simulations and experiments, because of the gap between experimentally relevant time scales and what can currently be achieved with simulations. The second motivation of this study is to consider the nanoparticle environment during the growth process, and especially the substrate effect on the structure in the case of nanoparticle formation by atom deposition from vapor phase[5]. A weakly interacting substrate, under ultra-high vacuum (UHV) conditions, is frequently considered as the most practical solution to form quasi-free nanoalloys.

The present work aims at assessing the competition between the equilibrium driving forces, including the substrate effect and the kinetic trapping, regarding the structure of Ag-Co nanoparticles during growth. The idea is therefore to follow the kinetics of the growth process of Ag-Co nanoparticles in two opposite modes of deposition on a substrate: direct sequential deposition (Ag atoms on an initial Co core) and reverse sequential deposition (Co atoms on an initial Ag core). These growth conditions can trap non-equilibrium arrangements due to lack of atomic mobility at moderate temperature, close to room temperature, as we have seen in the CoPt system[17]. However, the driving forces in the Ag-Co system have a strong tendency to converge in the same direction: a phase separation favoring Ag on the surface. The two questions that we try to answer in this paper are: What is the dominant mechanism in this highly immiscible system? What is the influence of the substrate in both growth sequences?

The originality of this study is the combination of atomistic simulations by molecular dynamics (MD) with experimental measurements, both having an almost atom-by-atom resolution in the growth sequence investigation. From an experimental point of view, previous studies[18] showed that the out-of-equilibrium configuration (the deposition of Co atoms on preformed Ag nanoparticles) leads to quite complex growth sequences. These sequences start with the incorporation of Co atoms in sub-surface positions and finally end with the formation of Co@Ag core-shell arrangements. The results, in good agreement with MD simulation, revealed structures with a Co core which is asymmetrically placed in the nanoparticle so that it is covered on one side by a very thin Ag shell. In the present paper, the direct sequence of deposition (the deposition of Ag atoms on preformed Co nanoparticles) more favorable to form directly a core-shell, is investigated as in the previous study, by in situ and time resolved X-ray Grazing Incidence scattering techniques at Small and Wide Angles (GISAXS and GIWAXS, respectively)[19,20]. Inspired by the experimental conditions concerning particle size, composition and growth sequence, equilibrium and growth atomistic simulations were done to obtain realistic structural models and to reveal the effects of the kinetics and of the substrate on the structure evolution. These simulations rely on a semi-empirical tight binding-based interatomic potential.

We chose here the parametrization for AgCo developed by the Ferrando group, which has already been successfully applied specifically to the nanoalloy system[18,21]. We go beyond earlier modelling by combining it with the Tersoff model that accounts here for the amorphous carbon substrate. Furthermore, we propose an implicit analytical model for the long-range dispersion forces that are an essential ingredient in models involving metal particles in close contact with a half space that is occupied by the substrate. The objective is two-fold : a first series of simulation investigates the equilibrium distribution of the particles with and without the presence of the substrate, which allows identifying its influence on the geometric properties of the particles. Secondly, atom-by-atom growth is simulated, thereby introducing kinetics effects that can be revealed by comparing with the first series of simulations.

The paper is organized as follows: section 2 gives the details of the experimental approach, the interatomic model, and the simulations protocols used in this study. In section 3, we present the simulation results and discuss to what extent they can be related to the experimental work (in the paper and Electronic Supporting Information (ESI †). Finally, the conclusion summarizes the main points while indicating limitations and our ideas on how to address the remaining open questions.

2 Methods

Before discussing the properties of the AgCo nanoalloy system, we first introduce the experimental and numerical methods for their determination. We begin with the experimental investigation (see also the ESI†) followed by the interatomic model that is used for the MD simulation, whose set up we also present at the end of the following section.

2.1 Experimental investigation

Experimentally, the nanoparticles were prepared at room temperature by vapor deposition of Co or Ag in UHV (2-5·10^{-10} mbar) on thermally oxidized Si(100) substrates covered with an amorphous carbon layer[22,23]. The surface of the nanoparticles can be considered as free, outside the interface with the substrate. The deposition rates are variable, which allows adjusting the final composition of the nanoparticles with values between 0.5 to 1·10^{15} atoms/cm^2/h (corresponding to a deposition rate of 5 to 10 ·10^{-3} monolayer/minute). Small-angle and wide-angle X-ray scattering experiments in grazing incidence (in GISAXS and GIWAXS, respectively) were carried out in real time during the atom deposition in situ in the UHV deposition set-up end-station on the SIXS beamline at SOLEIL synchrotron (see ESI † for details). GISAXS measurements provide morphological features of nanoparticle assembly as size, shape and correlation distance between particles on the substrate, while GIWAXS allows the determination of the atomic structure[17,19,20]. Considering the density of nucleation, the time resolution of the scattering spectrum recording was of one spectrum for each 5 atoms deposited in the capture area of each nanoparticle. In the reverse sequence, the initial Ag particles as seeds showed an icosahedral structure of an average size of 1.9 nm when Co atoms were deposited[18] (see ESI †). In the direct sequence, the initial Co particles showed a highly disordered structure, a mixture between an almost amorphous and icosahedral atom arrangement in the same range of size of 1.7 nm, then Ag atoms were deposited (see ESI †). These morphological and structural results were used as starting parameters for the modeling investigations. In the results and discussion

section 3 of this paper, experimental measurements of atom arrangement evolution during the deposition of the second metal, developed in ESI † part, are compared with the simulation results.

2.2 Interatomic model

The MD simulations we carry out to determine the equilibrium structures and the growth mechanisms of the particles are based on an atomistic semi-empirical model that we completed with an implicit analytical correction term to account for long-range dispersion forces.

The second moment approximation to the tight binding model (TB-SMA) [24] is widely used for transition metals, both in the form of bulk phases and nanoparticles [25–27]. The parametrization for Ag-Co [21], in particular, has been successfully used for the study of growth kinetics of AgCo nanoalloys by MD, which is very similar to what is simulated in the present contribution [18]. However, the objective of this work is to evaluate the influence of an amorphous carbon substrate on the structure and dynamics of deposited AgCo nanoalloys, and therefore it is necessary to combine the TB-SMA description with another model for carbon, which requires the possibility to include directional bonding. The Tersoff model stands as one of the fastest, yet realistic, descriptions for carbon materials with sp^2 and sp^3 bonds [28]. It has been shown that the TB-SMA model is a special case of the Tersoff model without the angular terms [29]. The TB-SMA model can thus be rewritten under the Tersoff form. This is however only true in the case of single element systems. In case of multi-element systems, the correspondence is not exact. Using the TB-SMA parameters for pure elements (Ag and Co) for the determination of the pure Tersoff parameters, and the mixed parameters (Ag-Co) for all the non-pure (Ag-Ag-Co, Ag-Co-Co, and permutations thereof) Tersoff parameters, a good agreement between the two descriptions can be achieved. In a typical configuration of a AgCo nanoalloy particle, the difference in energy between the TB-SMA potential and the Tersoff form is of less than 0.08 eV for the entire particle (<0.3 meV/atom), which is largely negligible. We opted here for this approach to obtain a unified model that accommodates both the metal and carbon part of the simulated system.

The interaction between the metal atoms (Ag and Co) with the carbon atoms of the substrate is described here by a simple Lennard-Jones model. We adopt here parameters introduced for the modelling of adsorption of metal clusters on carbon substrates: Neek and coworkers suggest $\sigma = 3.006$ Å, and $\varepsilon = 0.0301$ eV for Ag [30], while Popok and coworkers recommend $\sigma = 1.782$ Å, and $\varepsilon = 0.3$ eV for Co [31]. In both cases, we use a cut-off distance of 2.5σ.

Van-der-Waals forces are responsible for the adhesion of nanoparticles on semi-infinite substrates to a significant extent [32]. They affect the equilibrium shapes and surface diffusion of the adsorbed particles [33]. The reason for this is their long-range character combined with the infinite extension of the substrate. The modelling described above however does take into account only local interactions up to the respective cut-off distances. This problem also exists with DFT calculations relying on local or semi-local functionals, which is why several methods have been developed to correct for the missing long-range forces. One of the most straight-forwards ones that can also be easily combined with semi-empirical atomistic models is the Grimme approach: In particular, the D2 formulation [34] can be used as a basis for a dispersion correction for the present modelling:

$$E_{\text{disp}}^{\text{D2}} = -s_6 \sum_{i,j\neq i} \frac{C_6^{ij}}{r_{ij}^6} f_{\text{dmp}}^{ij}(r_{ij})$$

In this formulation, the contribution is calculated based on atomic pair distances r_{ij}, with the help of element-dependent C_6 coefficients, which are obtained as geometrical averages of coefficients for pure elements. We adopt the numerical values indicated by Grimme for the relevant elements: $C_6^{\text{Ag}} = 255.69$ eVÅ^6, $C_6^{\text{Co}} = 111.93$ eVÅ^6, and $C_6^{\text{C}} = 18.14$ eVÅ^6 [34]. The expression contains a short-range smooth cut-off function, f_{dmp}, which ensures that the dispersion contribution is only considered at distances that are not accounted for by a more precise short-range model to which the correction is added. The adjustable parameter s_6 is to be chosen as a function of the short-range model to which the dispersion correction is added. In our case, we found that $s_6 = 0.05$ well reproduced aspect ratios of Co and Ag particles deposited on amorphous carbon substrates as measured experimentally [35].

Despite being computationally expensive for large systems, this approach is not suitable for (semi-)infinite systems. Here, we opted therefore for integrating the contribution of substrate atoms that are not explicitly simulated, i.e. outside the simulation box, by assuming a substrate of uniform density ρ and semi-infinite extension. This approach was originally developed by Steele for adsorbed atoms on layered substrates modelled by Lennard-Jones interactions [36]. To do so, f_{dmp} is replaced by a sharp cut-off at the cut-off distance R^i of the Ag-C and Co-C interactions of the atomistic part of the model. This leaves us with the following expression for the implicit dispersion energy $E_{\text{disp}}^{\text{imp}}$ depending solely on the distance to the substrate surface d. This term is to be added to each of the transition metal atoms using the corresponding C_6 coefficients:

$$E_{\text{disp}}^{\text{imp}} = -\frac{s_6 C_6 \pi \rho}{2} \begin{cases} \frac{R-d}{R_4} + \frac{1}{3R^3} & \text{if } R-d>0 \\ \frac{1}{3d^3} & \text{else} \end{cases}$$

We note despite having used a sharp short-range cut-off function, the final expression is differentiable for all values of d which is essential for the usage with MD.

2.3 Simulation protocol

The geometric model for the amorphous carbon substrate used in simulations described in the following has been obtained beforehand by quenching a high-temperature random carbon system from 5000 K down to 300 K over a duration of 0.2 ns using the Tersoff potential [28]. We apply lateral periodic boundary conditions and reflective boundaries at the top and bottom to obtain a flat substrate surface without an unrealistic amount of dangling bonds. We use a slab thickness of 0.85 nm, which is more 0.1 nm more than the cut-off distance of the explicit atomistic part of the metal-carbon interatomic model. Laterally, the

substrate has a quadratic shape with an edge length of 5.3 nm, which is large enough to accommodate particles of 309 atoms of Ag and Co without them interacting with themselves via the periodic boundaries. The density was chosen to match the one of graphite, 2.4 g/cm^3, amounting to 2706 atoms. After the quenching, the system is equilibrated for 10 ps at 300 K keeping a bottom layer of 0.1 nm immobile in order to keep the system at a fixed vertical position in the later simulations. Throughout the subsequent simulations involving this substrate, its temperature was kept at 300 K using a Nosé-Hoover thermostat with a damping time of 100 fs, except the bottom layer of 0.1 nm which remained frozen. In these later simulations, the reflective boundary confining the substrate was moved to a position 5.3 nm above the substrate surface to have enough space to accommodate the metal particles.

2.4 Equilibrium simulation

The first objectives of this work is to study AgCo nanoalloys at equilibrium while evaluating the effect of the contact with an amorphous carbon substrate. Therefore, we carry out quenching simulations of a free Ag-Co gas mixture and the same gas mixture in contact with the amorphous carbon substrate obtained in the simulation discussed above. These simulations are initiated from a distribution of atoms at random positions at 3500 K, a temperature well above the boiling point of the two metals under investigation. The gas is cooled down to 300 K over 1 ns, which is long enough to obtain structures close to equilibrium. The simulations are then continued at 300 K for 0.1 ns to accumulate thermodynamic averages. The results shown in the following are based on the configurations from this last part of the simulation. The metallic gas contains 309 Ag atoms, and 10, 50, 100, 200, or 309 Co atoms. Simulations with the same composition, but exchanging Co for Ag atoms, are also carried out. The size of the particles is motivated here by the experimentally produced samples. Each of the simulations is run 450 times to obtain some statistics on possible structures sampled from the canonical ensemble.

2.5 Particle growth simulations by atom deposition

In order to better understand the growth dynamics, and the possibility of trapping the Ag-Co nanoalloy system in meta-stable states, we carry out simulations of atom by atom growth, of free particles and particles in contact with the mentioned amorphous carbon substrate allowing to assess the effect of the substrate on the growth dynamics. In this context, we consider growth on preformed 309-atom icosahedra of either Ag or Co, which were equilibrated at 300 K and 600 K over 100 ps with and without contact with the substrate. After equilibrating, while keeping the thermostat for the seed particle at 300 K and 600 K, atoms of the other metallic species (Ag in the case of the Co seed particle, and Co in the case of the Ag seed particle) were added every 50 ps at the top of the simulation box and random lateral positions. This is generally enough time for the atoms to be attached and diffuse on the growing particles. Atoms are added until equiatomic composition in terms of Ag and Co atoms, which leads to a total simulated time of 15.45 ns after equilibration. Their initial velocities were directed downwards with a speed of 0.5 nm/ps, corresponding roughly to the typical range of energies of atoms in atom-by-atom growth experiments[18]. The added particles were not directly subjected to the thermostat, but equilibrate rapidly with the substrate and metal atoms of the respective other atom type upon contact. Simulation runs for each of the situations, Ag on Co and Co on Ag growth, particle temperatures of 300 and 600 K, as well as the growth of free particles and particles on substrate were carried out.

3 Results and discussion

In the following, we discuss the results of the MD simulations together with the experimental data discussed in more detail in the ESI †. First, the distribution of particles at thermodynamic equilibrium is investigated, which allows thereafter to identify differences that occur when kinetic effects are considered. All simulations are carried out with and without the presence of an amorphous carbon substrate in order to be able to analyze its effect on the particles.

3.1 AgCo nanoalloys at thermodynamic equilibrium

To assess the distribution of properties of small AgCo nanoalloy particles, 450 independent simulation runs have been carried out. After a temperature quench that should bring the system close to the thermodynamic equilibrium, averages are accumulated in the canonical ensemble at 300K. Let us begin the discussion with the equimolar system containing 309 atoms of either species Ag and Co. In Fig. 1-a, a typical final simulation snapshots of the system with and without contact with the amorphous carbon substrate are shown. As expected, the core-shell structure with Co cores and Ag shells is recovered in these simulations, however, in most cases, especially in the case of the simulations including the substrate, the core is off-center and covered on one side by only a monoatomic layer of Ag atoms. This is indeed close to what is expected at equilibrium[11,12]. However, it should be noted that the particles we obtain here are somewhat more disordered as the true equilibrium state that is described in Refs. 11,12. The reason for this is the relatively high rate of quenching here, and it is thus difficult to discuss potential effects regarding crystallinity at this stage. Conversely, this has allowed many simulation runs to be carried out, and thus statistics to be obtained on the distribution of the global properties of the particles.

Unlike the investigations of free AgCo nanoparticles[10,12], where the main parameter of structural analysis is the relative distance between center of mass of silver and of cobalt, for the detection of substrate effects, the most pertinent parameters are rather the shape and mainly the orientation and position of center of mass of Ag and Co with respect to the substrate. In terms of particle shape, the most obvious is to monitor an asphericity parameter A[37]. Being always positive, A takes values close to zero for the most spherical shapes and can reach up to one when the shapes deviate strongly from them. Fig. 1-b reveals that on average, less spherical particles are formed on the amorphous carbon substrate, even though the effect is not very strong, and a significant number of simulation runs is required to be able to statisti-

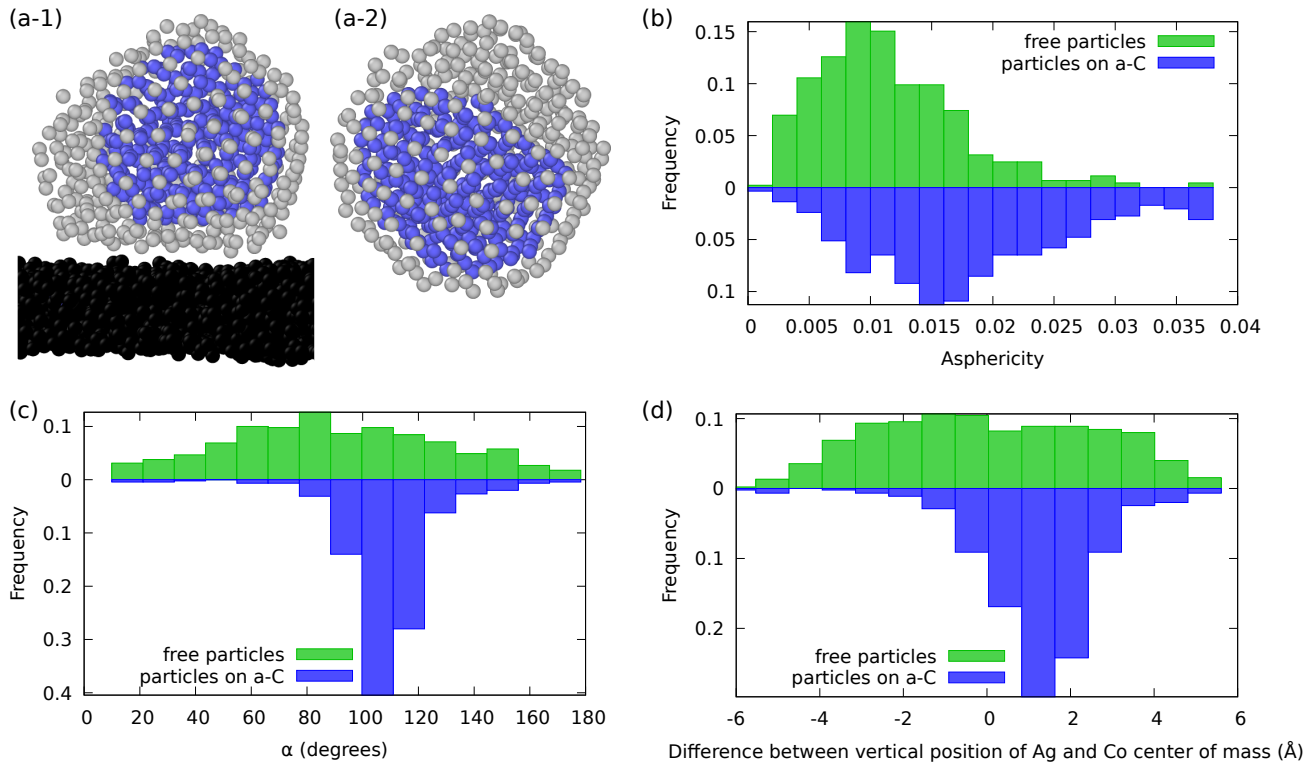

Fig. 1 (a) Typical final simulation snapshots of $Ag_{309}Co_{309}$ particles with (a-1) and without (a-2) contact with an amorphous carbon substrate at the end of the quenching simulations. (b) Asphericity of free particles and particles in contact with the substrate. (c) Orientation (see text) of the particles regarding the surface normal. (d) Relative vertical position of the Co and Ag center of mass.

cally observe the effect. This is because the particles follow the flat surface of the substrate at the contact area, and have thus a relatively large planar facet on one side of the particle. This facet usually consists of a monolayer of Ag atoms, on which the Co core is located.

The substrate also has an effect on the orientation of the particles, as evidenced by Fig. 1-c. The orientation is defined here as the angle α between the normal of the substrate surface and the vector pointing from the center of mass of the Co subsystem to the center of mass of the Ag subsystem. For example, in the case of the configuration represented in Fig. 1-a-1, while the surface normal points upwards, the vector from the Co to Ag center of mass points diagonally downwards, leading to a value of $\alpha = 100.1°$. In the simulations disregarding the substrate, the vector obviously has random orientations, but we note that this leads to a sinusoidal baseline distribution (instead of a uniform distribution) as shown in the upper histogram of Fig. 1-c. The distribution of the particles in contact with the substrate deviates very much from this baseline: most of the particles are oriented similarly to the particle on panel a-1, leading to a strong maximum of the distribution at around $\alpha = 100°$, with only small and few deviations from this value. This clearly indicates an effect of order that the substrate imposes on the distribution of the orientations of particles at equilibrium.

Similarly, the vertical separation of the Ag and Co center of mass has been calculated to determine which of the two metals is closer to the substrate. Positive values indicate particles where the Co center of mass is further away from the substrate. In the baseline case, without the substrate, the distribution of the quantity is expected to be symmetrical with respect to zero, which is observed here (see upper histogram of Fig. 1-d). For free particles, the distribution is rather flat, meaning that large separations of the centers of mass of the two metals are preferred, which reflects the fact that many of the particles are in quasi-Janus configuration, as shown previously in Ref. 12. In case of these free $Ag_{309}Co_{309}$ particles, this distance is typically of the order of 2–3 Å. In contact with the substrate, the Ag center of mass is slightly (1.5–2 Å) closer to the substrate surface than the center of mass of the Co core. In case of perfect core-shell particles, one would expect equal separation of the two centers of mass from the substrate surface. This discrepancy is explained by the fact that Ag atoms in excess of a monoatomic surface layer on the Co core accumulate at a position in contact with the substrate. This is despite the fact that also the Co core is usually rather close to the substrate surface - separated by only one monolayer of Ag.

Let us now turn the discussion towards the effect of chemical composition of the particles on the quantities discussed above. In a first step, we consider their equilibrium distribution in order to be able to identify kinetic effects present in the growth simulations discussed in section 3.2. As shown in Fig 2-a, regarding asphericity, it can be noted that the free particles remain in a spherical configuration regardless of chemical composition. Also in case of the particles in contact with the substrate, the shape of the particles does not seem to be affected much by the chemical composition of the particles, with slightly more spherical shapes when the composition approaches pure Ag or pure Co particles.

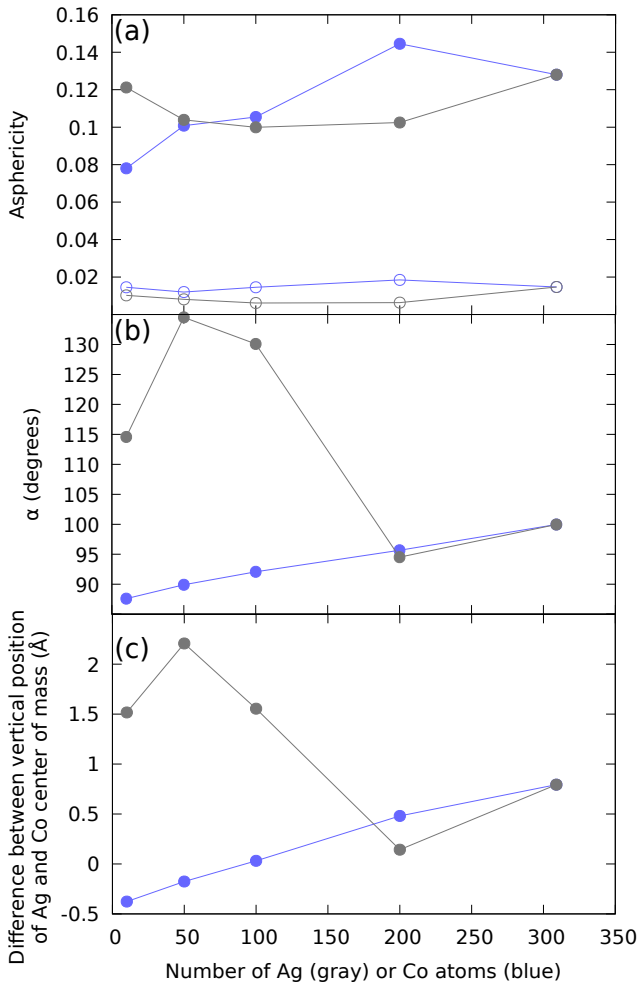

Fig. 2 Particle geometry and orientation at thermodynamic equilibrium at 300K for free particles (open circles) and particles in contact with an amorphous carbon substrate (full circles) as a function of chemical composition. Particles always contain 309 atoms of one metal (Ag or Co) and a variable number of atoms of the respective other species, represented on the x-axis. (a) Particle asphericity. (b) Particle orientation (same definition as Fig. 1-c). (c) Relative vertical position of the Co and Ag center of mass.

However, these particles in contact with the substrate are clearly less spherical. The contact with the substrate remains thus the most important factor affecting particle shape.

Secondly, the orientation of the particles on the substrate surface is assessed with the help of α (same definition as before), the angle between the substrate normal and the vector from the Co center of mass to the Ag center of mass. By increasing the amount of Co of a Ag majority particle (blue curves), the angle increases from values close to 90° to about 100° at equicomposition (Fig. 2-b). Angles close to 90° correlate here with particles where the center of mass of the Co core is roughly at the same distance from the substrate surface as the center of mass of the Ag shell. This fact is also reflected in Fig. 2-c, where the vertical separation of the two centers of mass vanishes at small Co content. This means, in these cases, there is more than one monolayer of Ag atoms separating the core from the substrate.

Co majority particles (gray curves) with some Ag atoms usually have their cores separated from the substrate by the few Ag atoms present in the system. This makes the vector from the Co to the Ag center of mass pointing in the direction of the substrate, leading to larger values of α in Fig. 2-b. Similarly, Fig. 2-c shows that the vertical separation of the center of masses of the two subsystems reaches a maximum at these compositions with only a few Ag atoms. We use these baseline equilibrium simulations for comparison when discussing the simulations of particle growth in the following section.

3.2 Particle growth kinetics

To fully understand our experimental results and growth dynamics, we used MD with atom deposition to simulate particle growth. Particles are grown by Ag or Co atom-by-atom addition at random positions at the top of the simulation box and directed towards the substrate with an initial Co or Ag particle (as seeds), respectively. We performed this growth for free particles and carbon-supported particles to evaluate the influence of the substrate and to simulate the experimental conditions as well as possible.

3.2.1 Ag on Co

The experimental results show the formation of icosahedral structures for pure Co particles for which the deposition of Ag atoms is carried out. A Co icosahedron of 309 atoms ($Ih_{Co_{309}}$) has a diameter of 1.9 nm, close to the experimental average size (see section 2.1 and ESI †). Before the Ag growth process, the icosahedral Co seed was relaxed at 300 K. Ag atoms were then deposited atom-by-atom from the top of the simulation box onto an area a_d of deposit of 5.3 nm by 5.3 nm containing the Co seed particle at a rate of 1 atom every 0.05 ns. With MD, it is not possible to reach experimental growth timescales (experimental timescales are by a factor of $4{\cdot}10^{-12}$ slower) due to prohibitive computational cost.

The direct Ag growth process is studied at 300 K and 600 K ; corresponding snapshots of growth sequences are shown in Fig. 3-a and Fig. 3-b respectively. These structures do not correspond to chemical equilibrium across the full compositional range. The nanoparticles keep icosahedral shape until the entire surface is covered with Ag atoms. When the Ag atoms reach the nanoparticle, they diffuse on the surface for some time to form many small

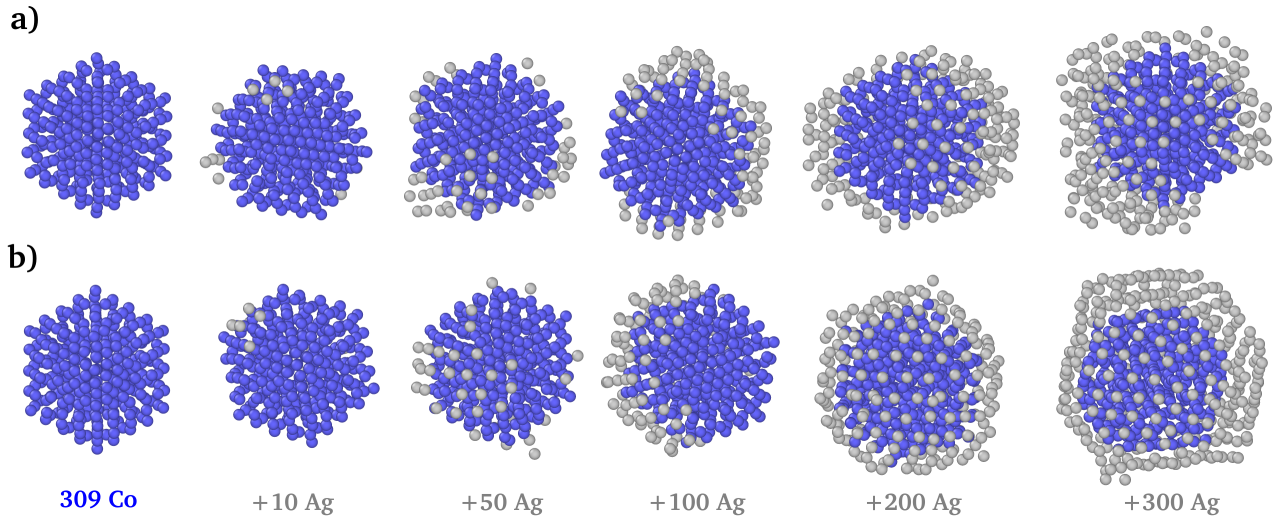

Fig. 3 Snapshots of the growth of Ag on an initial free Co nanoparticle($Ih_{Co_{309}}$) at 300K (a) and 600K (b). The snapshots are taken at different stages of growth until 50% Ag content. Co and Ag atoms are represented as blue and gray spheres, respectively.

Ag patches. As the number of deposited Ag atoms increases, after diffusion, a single 2D domain of Ag atoms (Ag layer) forms. This can be explained by the fact that Ag atoms seek to create the maximum number of possible bonds while remaining at the surface (the most favorable position of Ag atoms is the surface due to its large size and low surface energy compared to Co). At 600 K and by continuing the deposition until a composition of 40% of Ag, Ag atoms completely cover the surface of the Co particle, forming a core/shell(Co@Ag) structure which is in good agreement with the experimental results concerning equilibrium states[35]. Conversely, at 300 K (Fig. 3-a), Ag atoms do not diffuse on the surface of the Co particle due to reduced mobility at this lower temperature and rather stick to other Ag atoms to form a second layer of Ag on the Co particle.

We shift the discussion now to the Ag atom-by-atom growth on Co particles supported on an amorphous carbon substrate in order to evaluate potential effects of the latter. On a 5.3 nm by 5.3 nm substrate with a thickness of 1 nm, a 309-atom icosahedral Co particle is deposited. The system composed of the substrate and particle are relaxed at 300 K. As with the free particles, we study the growth process at 300 K and 600 K at the same deposition rate, but with particles in contact with the carbon substrate. Snapshots of growth sequences at 300 K and 600 K are shown in Fig. 4-a and Fig. 4-b) respectively.

From Fig. 4, as with the free particles, it can be seen that the nanoparticles keep the icosahedral shape until the entire surface is covered in Ag. The deposited Ag atoms either land on top of the Co cluster or on the substrate. While being mostly stationary on the substrate, the initial Co icosahedron undergoes some rocking motion: sometimes having just one edge in contact with the substrate, while at other times presenting a full facet to the substrate (as shown on the initial snapshot). If landed on the substrate, the deposited Ag atoms diffuse to reach the clusters and stick to them. At 600 K, the Ag atoms that land on top of the Co particle diffuse on its surface to join other Ag atoms which are bonded with both Co and C atoms. At 300 K, the Ag atoms remain stationary at the point of first contact with the Co seed particle. This may however only be a result of the slower kinetics at 300 K and the short simulation duration, and thus not be observed in experiments (see ESI †), which is why we included the simulations at 600 K. Ag first covers the surface of the Co particle at the contact area with the substrate and then gradually fills the entire surface of the seed particle to form a core-shell structure. At 40% Ag, tens of Ag atoms cluster on the substrate in contact with the core-shell particle, changing its orientation. At 50% of Ag finally, we obtain a quasi-Janus structure similar to what has been obtained at equilibrium.

At 40% Ag and out-of-equilibrium growth, experimental evidence points to Janus structures at 300 K which is not reproduced with the current simulations. At 50% of Ag, a second layer of Ag begins to form on the surface of the Co particles and at equilibrium quasi-Janus structures are obtained similar to the structures found here by the simulations.

3.2.2 Co on Ag

As in the previous section 3.2.1 and with the same growth rate, reverse growth of Co atoms was performed on the free Ag 309-atom icosahedron of 2.1 nm close to the experimental average size (see section 2.1 and ESI †). Fig. 5-a and Fig. 5-b, show the growth sequences at 300 K and 600 K, respectively. The 309-atom Ag nanoparticle mostly keeps its icosahedral shape upon deposition of Co up to about 20% of Co content at 300 K in good agreement with the experiments[18] and 5% of Co content at 600 K. At 600 K, when a Co atom arrives at the surface of the particle, it diffuses into the subsurface which is the most favorable position for a Co atom when exchanged with a Ag atom that consequently moves above the original surface. The segregation of Co in subsurface condition has been confirmed by many theoretical[11,12] and experimental studies[18]. By increasing the number of deposited Co atoms, Co clusters accumulate in subsurface condition through subsurface diffusion of Co atoms. The Co domain forms because of the much stronger Co-Co interactions compared

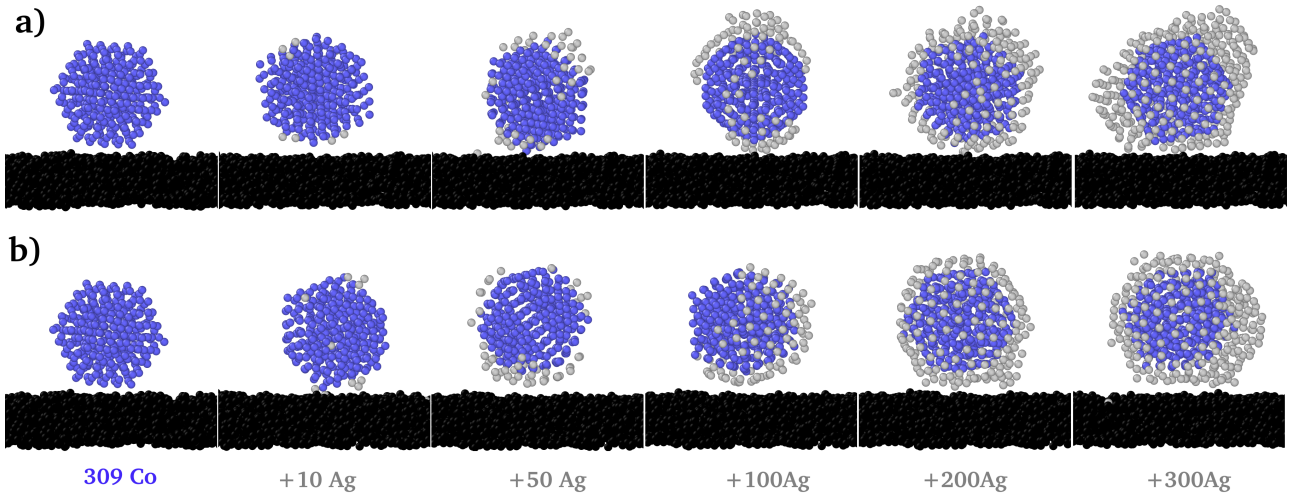

Fig. 4 Snapshots of the growth of Ag on an initial Co nanoparticle($Ih_{Co_{309}}$) supported on an amorphous carbon substrate. The snapshots are taken at different stages of growth until 50% Ag atom content. Co and Ag atoms are represented as blue and gray spheres, respectively. (a) Sequence at 300 K, (b) Sequence at 600 K

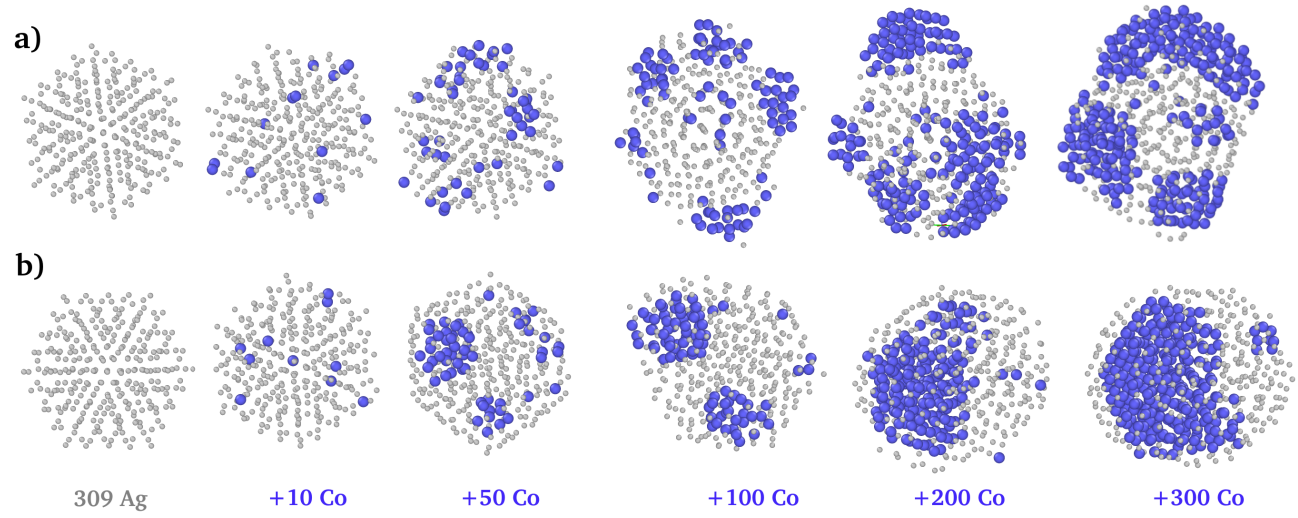

Fig. 5 Snapshots of the growth of Co on an initial Ag nanoparticle($Ih_{Ag_{309}}$) at 300 K (a) and 600 K (b). The snapshots are taken at different stages of growth, of up to 50% Ag atom content. Co and Ag atoms are represented as blue and gray spheres, respectively.

to Ag-Co interactions. After the deposition of 300 atoms of Co, quasi-Janus structures are obtained, which is in good agreement with earlier simulation results [10,11,18] and consistent with experiments [18]. Continuing the deposition with up to 600 Co atoms leads to Co@Ag core/shell structures (see ESI †and Ref. 18). At 300 K and at low Co concentration, the majority of the Co atoms remain on the surface of the particle and the only a minority diffuses into the subsurface. By increasing the Co content and because of the low mobility of Co at 300K, the formation of Co clusters on the surface of the particle is observed. Some of these Co clusters may however also diffuse towards the center of the Ag particle. Co clusters are thus partially surrounded by Ag when depositing up to 300 Co atoms.

In Fig. 6, the growth by Co atoms on an Ag particle supported by a carbon substrate can be examined. During deposition, the Co atoms arrive either on the particle or on the substrate. The atoms which are deposited on the substrate remain there with very limited diffusion. In particular, these atoms are not mobile enough to join the particle, as it was the case with the Ag atoms. This is explained by the much stronger interaction of Co-C as compared to Ag-C. The Co atoms, which are directly deposited on the Ag particle, diffuse into the subsurface as in the case of the free particles. At 600 K (Fig.6-b), the growth proceeds similarly to the free particles, with some modulations: Firstly, at around 300 deposited Co atoms, the layer of Ag which is in contact with the carbon becomes flat. Secondly, the particles of quasi-Janus type assume mostly an fcc lattice structure which is in good agreement with experimental observation at the same temperature, but larger size of particles (data not shown) due to the interaction with the substrate. At 300 K (Fig.6-a), the growth resembles the behavior of the free particles even more, the only difference being that the structure remains icosahedral until the end of the Co deposition. In comparison with the results at 600 K, at 300 K the kinetics is very much reduced, and the Co atoms cluster together at the particle surface before migrating to the subsurface. It can be speculated that, given enough time, the structures obtained at 300 K will eventually evolve towards those obtained at 600 K.

4 Conclusions

Experimentally, we have performed the growth of nanoparticles (Co on Ag or Ag on Co) by atom-by-atom deposition of the metals on an amorphous carbon substrate. The particles were then analyzed by different X-ray scattering techniques. These experimental results were the starting point of molecular dynamics simulation study, revealing the equilibrium structure of the particles and influence of the substrate. Furthermore, growth of the particles was simulated to assess kinetic effects in conjunction with substrate effects. Both growth sequences, direct: Ag on Co, and reverse: Co on Ag were addressed.

The most important driving factor for the AgCo nanoalloy system is its tendency for demixing, which we observe at equilibrium, as well as in both orders of growth (Ag on Co, as well as Co on Ag). At the end of the growth, stable core-shell and quasi-Janus structures are thus obtained.

At equilibrium, a quasi-Janus structure is obtained at equimolar composition. Comparing the behavior of the free particle with particles supported by an amorphous carbon substrate, two effects can be discerned: the asphericity increases and the orientation of the particles, as quantified by the vector pointing from the Co to the Ag center of mass, tilts towards the substrate.

Concerning particle growth, in both orders of deposition, we find that the kinetics is reduced at 300 K in comparison to the behavior at 600 K. We speculate here, and this is the motivation for our simulations at 600 K, that the structures obtained at 300 K would eventually evolve towards what we observe at higher temperature, which therefore gives a glimpse of what we expect to happen at experimental timescales. In case of Ag deposition on Co seeds, the Ag atoms remain on the surface, which is reasonable because the most favorable position of Ag is indeed the particle surface, as determined in our assessment of the equilibrium configuration. It can be rationalized by the low surface energy of Ag atoms and their large size compared to the Co atoms. The direct growth in this order, Ag on Co, yields thus first Co@Ag core-shell structures that evolve towards quasi-Janus structure as more and more Ag is deposited. In the reverse order of growth, Co on Ag, the deposited Co atoms exchange position with subsurface Ag atoms, leaving us with particles presenting an Ag surface and Co subsurface clusters. Continuation of atom-by-atom growth eventually leads to quasi-Janus chemical ordering when the particle composition reaches 50% of Co. In terms of substrate effect, we note that similar quasi-Janus particles are obtained, but having a more crystalline cubic (fcc) structure which should be compared to the free particles which are more disordered. The amorphous carbon substrate thus favors crystallinity of the bimetallic nanoalloys.

According to our experimental results, in the case of Co deposition on Ag, Co aggregates form inside the Ag matrix. Therefore, a Co@Ag core-shell structure is obtained at the end of the growth process. For deposition of Ag on Co, our experimental work is indicative of the formation of a Janus structure, which is not exactly reproduced in our simulations where we obtained rather an atom arrangement closer to a core-shell than to a Janus structure at a composition of 40% Ag. We suspect that this points to a shortcoming in our modelling: the carbon metal interactions (especially Co-C, but also Ag-C) are likely to be underestimated compared to the interactions within the transition metal subsystem (Ag-Ag, Co-Co, and Ag-Co). Furthermore, our approach of modelling these interactions with a simple Lennard-Jones potential neglects some aspects of the local atomic environments, in particular angular bonding, which still may play a certain role for the stabilization of the particles on the substrate. Therefore, for a more precise study of these local effects, we would suggest the usage of models that account better for atomic environments, such as TB-SMA or Tersoff, also for the carbon-metal interactions.

Author Contributions

AH, DF and RF contributed to write the original draft; CA, AC and YG contributed to review & editing. All authors contributed to the investigation: CA, YG, AC, PA for experimental results and analysis; AH, DF and RF for calculation and simulation interpretation. The electronic supplementary information (ESI) concerning X-ray scattering measurements was written by PA. All the manuscript

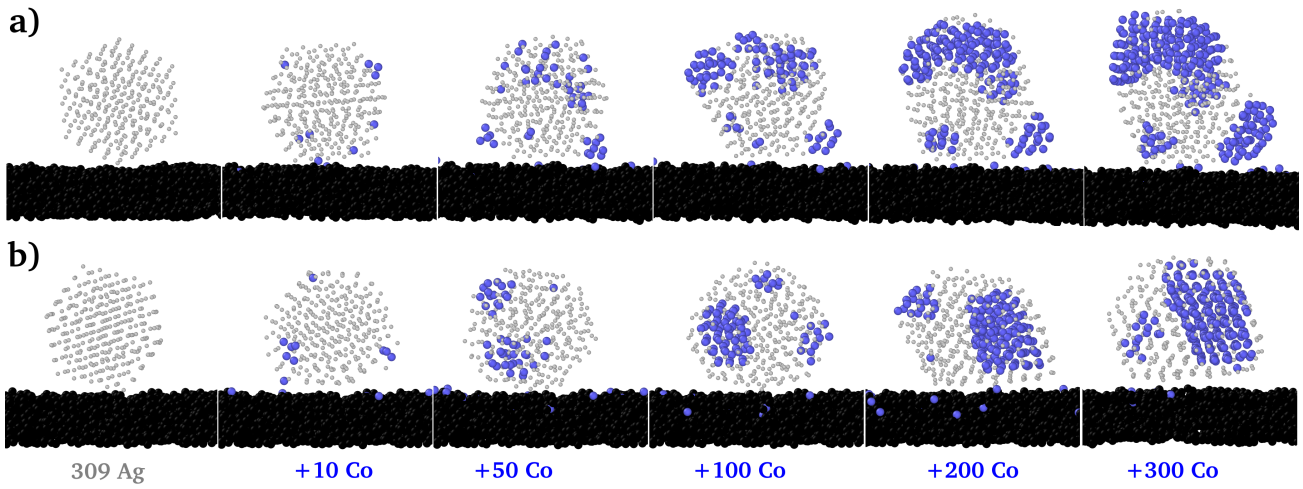

Fig. 6 Snapshots of the growth of Co on an initial Ag nanoparticle($Ih_{Ag_{309}}$) supported on an amorphous carbon substrate. The snapshots are taken at different stages of growth of up to 50% Ag content. Co and Ag atoms are represented as blue and gray spheres, respectively. (a) Sequence at 300 K, (b) Sequence at 600 K

and ESI were carefully and critically reviewed by all the authors.

Conflicts of interest

There are no conflicts to declare.

Acknowledegments

We would like to thank our former and present Ph.D. students especially, Asseline Lemoine, for his fruitful contribution to the experimental part of this work. The authors are grateful to Diana Nelli (Universita di Genova) and Jérome Creuze (Université Paris Saclay) for helpful discussions. Finally, the authors acknowledge SOLEIL (Gif-sur-Yvette, France) synchrotron facility for synchrotron radiation access and the SixS beamline team, in particular Alina Vlad and Benjamin Voisin for technical help, and we also acknowledge support from the Fédération CaSciModOT (CCSC Orléans-Tours, France) that gave us access to the Région Centre computing grid. This work was supported by the international research network IRN Nanoalloys of CNRS and the French Region council Centre-Val de Loire, Contract No. 201100070575.

References

1 R. Ferrando, *Structure and Properties of Nanoalloys*, Elsevier, 2016, vol. 10.
2 R. Ferrando, J. Jellinek and R. L. Johnston, *Chem. Rev.*, 2008, **108**, 845–910.
3 J. Jellinek, *Faraday Discuss.*, 2008, **138**, 11–35.
4 F. Calvo, *Phys. Chem. Chem. Phys.*, 2015, **17**, 27922–27939.
5 P. Andreazza, V. Pierron-Bohnes, F. Tournus, C. Andreazza-Vignolle and V. Dupuis, *Surf. Sci. Rep.*, 2015, **70**, 188–258.
6 Chen, B. C. Curley, G. Rossi and R. L. Johnston, *J. Phys. Chem. C*, 2007, **111**, 9157–9165.
7 M. Zhang and R. Fournier, *Journal of Molecular Structure: THEOCHEM*, 2006, **762**, 49–56.
8 J. M. Martinez De La Hoz, R. Callejas Tovar and P. B. Balbuena, *Mol. Simul.*, 2009, **35**, 785–794.
9 G. Rossi, A. Rapallo, C. Mottet, A. Fortunelli, F. Baletto and R. Ferrando, *Phys. Rev. Lett.*, 2004, **93**, 105503.
10 I. Parsina and F. Baletto, *J. Phys. Chem. C*, 2010, **114**, 1504–1511.
11 K. Laasonen, E. Panizon, D. Bochicchio and R. Ferrando, *J. Phys. Chem. C*, 2013, **117**, 26405–26413.
12 D. Bochicchio and R. Ferrando, *Phys. Rev. B Condens. Matter*, 2013, **87**, 165435.
13 F. Calvo, A. Fortunelli, F. Negreiros and D. J. Wales, *J. Chem. Phys.*, 2013, **139**, 111102.
14 F. Calvo, *Eur. Phys. J. Appl. Phys.*, 2022, **97**, 16.
15 J. A. De Toro, J. P. Andrés, J. A. González, J. P. Goff, A. J. Barbero and J. M. Riveiro, *Phys. Rev. B Condens. Matter*, 2004, **70**, 224412.
16 R. Sachan, S. Yadavali, N. Shirato, H. Krishna, V. Ramos, G. Duscher, S. J. Pennycook, A. K. Gangopadhyay, H. Garcia and R. Kalyanaraman, *Nanotechnology*, 2012, **23**, 275604.
17 H. Khelfane, C. Andreazza-Vignolle, A. Y. Ramos, J. Penuelas, T. Sauvage and P. Andreazza, *Eur. Phys. J. Appl. Phys.*, 2022.
18 P. Andreazza, A. Lemoine, A. Coati, D. Nelli, R. Ferrando, Y. Garreau, J. Creuze and C. Andreazza-Vignolle, *Nanoscale*, 2021, **13**, 6096–6104.
19 P. Andreazza, *Nanoalloys: Synthesis, Structure and Properties*, Springer London, London, 2012, pp. 69–112.
20 J. Penuelas, P. Andreazza, C. Andreazza-Vignolle, C. Mottet, M. De Santis and H. C. N. Tolentino, *Eur. Phys. J. Spec. Top.*, 2009, **167**, 19–25.
21 G. Rossi, G. Schiappelli and R. Ferrando, *J. Comput. Theor. Nanosci.*, 2009, **6**, 841–848.
22 J. Penuelas, C. Andreazza-Vignolle, P. Andreazza, A. Ouerghi and N. Bouet, *Surf. Sci.*, 2008, **602**, 545–551.
23 P. Andreazza, C. Mottet, C. Andreazza-Vignolle, J. Penuelas, H. C. N. Tolentino, M. De Santis, R. Felici and N. Bouet, *Phys. Rev. B Condens. Matter*, 2010, **82**, 155453.
24 F. Cleri and V. Rosato, V, *Phys. Rev. B Condens. Matter*, 1993, **48**, 22–33.

25 A. Chmielewski, J. Nelayah, H. Amara, J. Creuze, D. Alloyeau, G. Wang and C. Ricolleau, *Phys. Rev. Lett.*, 2018, **120**, 025901.
26 A. Lopes, G. Tréglia, C. Mottet and B. Legrand, *Phys. Rev. B Condens. Matter*, 2015, **91**, 035407.
27 D. Cheng, S. Yuan and R. Ferrando, *J. Phys. Condens. Matter*, 2013, **25**, 355008.
28 J. Tersoff, *Phys. Rev. B Condens. Matter*, 1989, **39**, 5566–5568.
29 D. W. Brenner, *Phys. Rev. Lett.*, 1989, **63**, 1022–1022.
30 M. Neek-Amal, R. Asgari and M. R. Rahimi Tabar, *Nanotechnology*, 2009, **20**, 135602.
31 V. N. Popok, S. Vučković, J. Samela, T. T. Järvi, K. Nordlund and E. E. B. Campbell, *Phys. Rev. B Condens. Matter*, 2009, **80**, 205419.
32 A. Ambrosetti, P. L. Silvestrelli and A. Tkatchenko, *Phys. Rev. B Condens. Matter*, 2017, **95**, 235417.
33 G. D. Förster, F. Rabilloud and F. Calvo, *Phys. Rev. B Condens. Matter*, 2015, **92**, 165425.
34 S. Grimme, *J. Comput. Chem.*, 2006, **27**, 1787–1799.
35 A. Lemoine, *PhD thesis*, Université d'Orléans, 2015.
36 W. A. Steele, *Surf. Sci.*, 1973, **36**, 317–352.
37 F. Calvo, F. Chirot, F. Albrieux, J. Lemoine, Y. O. Tsybin, P. Pernot and P. Dugourd, *J. Am. Soc. Mass Spectrom.*, 2012, **23**, 1279–1288.

Electronic Supplementary Information

Combined atomistic simulations to explore metastability and substrate effects in Ag-Co nanoalloy systems

A. Hizi[1], D. Forster[1], R. Ferrando[2], Y. Garreau[3,4], A. Coati[3], C. Andreazza-Vignolle[1], P. Andreazza[1*],*

**Corresponding Authors, georg-daniel.forster@univ-orleans.fr, pascal.andreazza@univ-orleans.fr*

1 Université d'Orléans, CNRS, ICMN UMR7374, 1b rue de la Férollerie, F-45071 Orléans, France
2 Università di Genova, Dipartimento di Fisica, Via Dodecaneso 33, Genova, I16146, Italy
3 Synchrotron SOLEIL, L'Orme de Merisiers, F-91192 Gif-sur-Yvette, France
4 Université Paris Cité, CNRS, Laboratoire Matériaux et Phénomènes Quantiques UMR7162, F-75013 Paris, France,

Synchrotron radiation experimental procedure

In-situ Grazing Incidence Small Angle X-ray Scattering (GISAXS) and Grazing Incidence Wide Angle X-ray Scattering (GIWAXS) measurements were carried out at the SOLEIL Synchrotron in Gif-sur-Yvette, France, at the SIXS beamline [1,2]. The photon energies and the incidence angle were chosen to reduce the absorption-induced fluorescence effect and to optimize the analysis depth to some nanometers [3]. The sample detector distance was chosen for each x-ray energy to adjust the q range of the collected signal in the reciprocal space. All GIWAXS signals were collected with an XPAD 2D detector to scan the scattered intensity in a large reciprocal space area, while for the GISAXS measurements, the 2D Mar CCD detector was used and located in a fixed position in the small reciprocal space area close to the direct beam. The GISAXS and GIWAXS detectors were calibrated in terms of detection uniformity, spatially and energetically.

The geometry of the scattering data collection is defined at a fixed grazing incidence α_i [3,4]: The scattered intensity is recorded as a function of the out-of-plane angle α_f with respect to the substrate surface and of the in-plane angle $2\theta_f$ (Fig. S1). For GIWAXS, the exit angle α_f is fixed and the scan angle is $2\theta_f$. The components of the momentum transfer $\mathbf{q} = \mathbf{k_i} - \mathbf{k_f}$, (scattering vector) defined by the incident k_i and the scattered k_f wave vectors are $q_x = k_i (\cos\alpha_f \cos 2\theta_f - \cos\alpha_i)$, $q_y = k_i (\cos\alpha_f \sin 2\theta_f)$ and $q_z = k_i (\sin\alpha_f + \sin\alpha_i)$ in the laboratory frame, x and y in the surface substrate plane and z out-of plane (y perpendicular to the incident beam). For GISAXS, the intensity is recorded in q_y and q_z on the 2D detector.

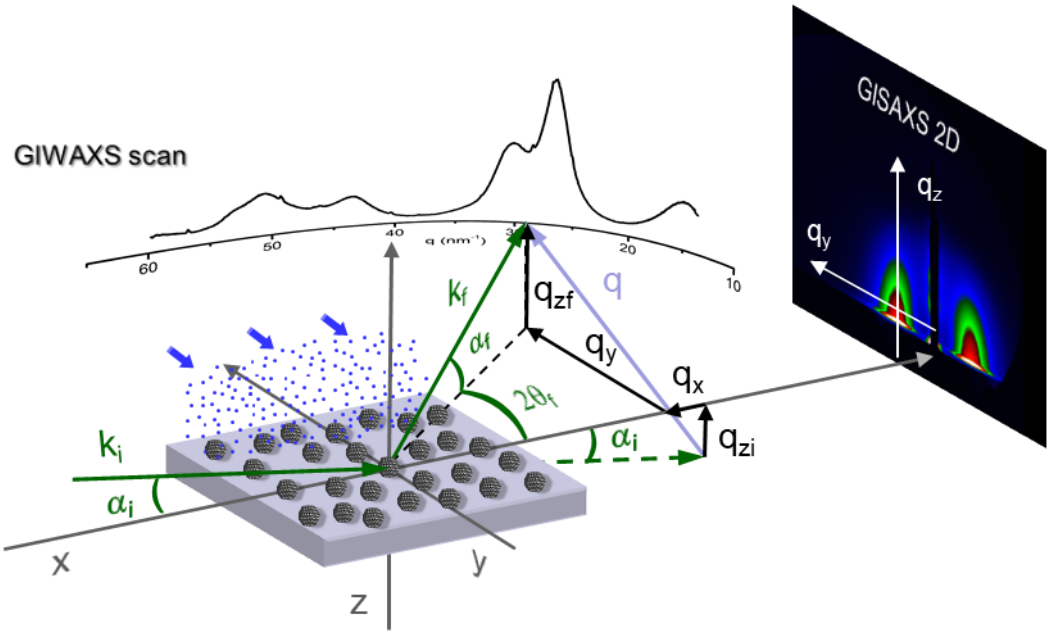

Figure S1: Strategy of the scattering data collection with an incident beam of wavevector $\mathbf{k_i}$, a scattered beam in the direction $\mathbf{k_f}$, with respect to the sample and the 2D GISAXS and 0D GIWAXS detection geometry (corresponding to q_z - q_y range, and q range profiles respectively).

Concerning the GISAXS data analysis: two cuts of intensity, *i.e.* 1D profiles, in the q_z and q_y, directions were extracted from a 2D GISAXS pattern as in Ref. [2]. The two perpendicular experimental cuts selected in the lobe intensity region (white lines) in Fig. S1 were simultaneously fitted with a dedicated code, the IsGISAXS software [4]. The simulations were made for a distribution of nanoparticles of weakly-truncated spherical shapes, to consider of the weak interactions between the deposited metals and the substrate [3,4]. According to the NPs organization on the substrate, the inter-particles correlation function was calculated using the Local Monodisperse Approximation (LMA), and a 1D-paracrystal organization model [4,5]. The adjustable parameters of the simulations were the NPs diameter D, the aspect ratio H/D (where H is the NPs height), the relative distribution of diameters σ(D)/D, the inter-particles distance Λ, and its standard deviation σ(Λ)/Λ [5].

Concerning the GIWAXS data analysis: the 1D experimental scattering profile was compared with simulated patterns obtained from a calculated model cluster on the basis of the Debye equation [2,6,7] and considering the set-up geometry using a dedicated custom software [8]. Preliminarily, a reference pattern from a substrate region without particle was measured in the same conditions, and was subtracted from the deposited nanoparticle sample pattern. The model clusters were obtained from molecular dynamics simulations with atomic displacements and chemical species exchanges of Co and Ag atoms in the canonical ensemble, using a semi-empirical potential as explained in the main text. A weighted sum of the intensities from several sizes or structures was used to fit the WAXS patterns considering the size distribution coming from GISAXS results [3].

Experimental investigation of Co deposition on Ag core

The in situ GIWAXS and GIWAXS results [2] reveal the time-resolved structural evolution during the Ag and Co depositions (see Fig. S2). For low amount of deposited Co atoms, we observe an incorporation of Co atoms over interatomic distances close to that of Ag, while the structure of the initial Ag particles is mostly kept as it is. At the highest amounts of Co, the Ag atoms lose their coherence, corresponding to a shorter distance order in the initial Ag domains, while domains of Co are created close to the interatomic distance of Co bulk (within 1% of the bulk lattice spacing). These observations from the initial Ag (average size of 1.9 nm) until a composition of about 70% Co atoms is reached, which reflect a progressive reduction of the coherence length in Ag domains and of the number of Ag neighbors, and also a higher local structural disorder, agree with a progressive formation of a core-shell Co@Ag particle by incorporation and agglomeration of Co atoms in the Ag nanoparticles.

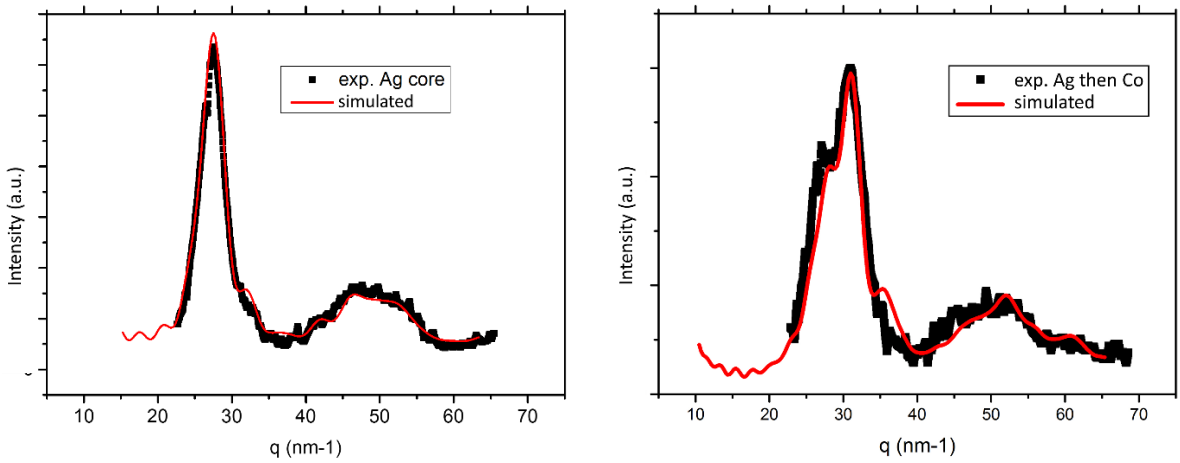

Figure S2 : GIWAXS spectra : (left) Initial Ag particle, and (right) Ag particle after Co deposition (until the AgCo2 composition), associated respectively with the simulated spectrum (red line) coming (left) from icosahedral distribution of Ag models centered on 309 atoms in size, and (right) from a Co-core/Ag-shell model of $Ag_{309}Co_{600}$ atoms.

Experimental investigation of Ag deposition on Co core

As previously, in situ scattering measurements showed that Ag nucleation does occur on the initial Co islands (average size of 1.7 nm), but does not lead to a core-shell configuration (see Fig. S3). After the deposition of Ag atoms on Co particles until about a composition of 40% Ag atoms, the GIWAXS measurements showed the formation of a silver domain associated with the initial Co core, as revealed by the GISAXS analysis of the size increase with the same density of particles. The kinetics of formation is most certainly the following: i) nucleation of Ag at the substrate/Co island interface, ii) growth of the Ag domain(s) on these nucleation sites, leading to a "pseudo-Janus" type configuration that minimizes the number of Ag-Co bonds that are energetically more unfavorable than Ag-Ag bonds. The presence of a substrate combined with kinetic considerations could be the origin of this behavior, and not only the immiscibility

between Co and Ag, that control the mechanism of Ag formation on Co islands leading to a final multidomain structure.

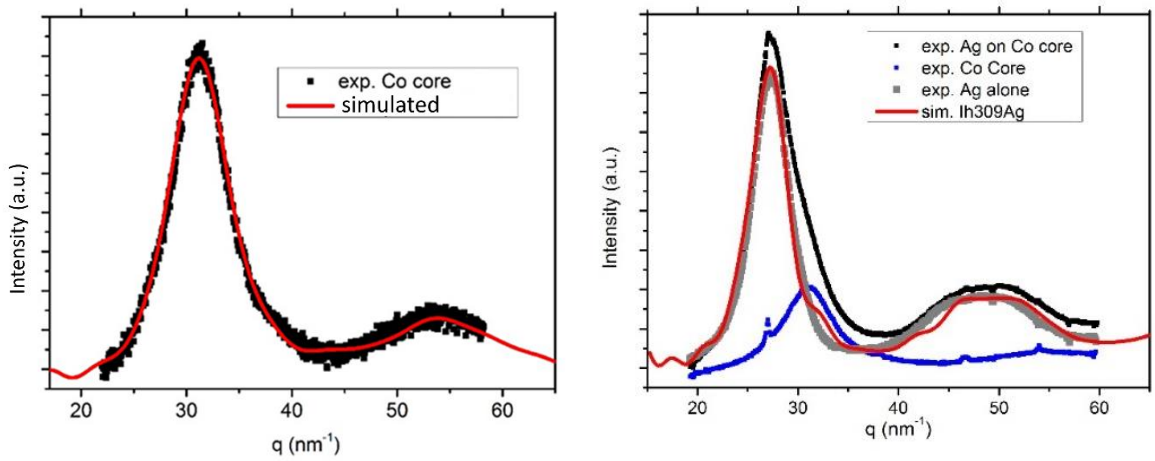

Figure S3 : GIWAXS spectra : (left) Initial Co particle, and (right) Co particle after Ag deposition (until the AgCo composition), associated respectively with the simulated spectrum (red line) coming (left) from amorphous and icosahedral distribution of Ag models centered on 1.7 nm in size, and (right) from the Co-Ag biparticle model with a Ag domain of icosahedral distribution of Ag models centered on Ag_{309} atoms.

References

[1] Coati, A., Chavas, L. M. G., Fontaine, P., Foos, N., Guimaraes, B., Gourhant, P., Thompson, A. Status of the crystallography beamlines at synchrotron SOLEIL, European Physical Journal Plus, 132(4) (2017).

[2] Andreazza P., Lemoine A., Coati A., Nelli D., Ferrando R., Garreau Y., Creuze J., Andreazza-Vignolle C., From metastability to equilibrium during the sequential growth of Co-Ag supported clusters: a real-time investigation, Nanoscale 13, 6096 – 6104 (2021).

[3] Andreazza P. (2012) Probing Nanoalloy Structure and Morphology by X-Ray Scattering Methods. In: Alloyeau D., Mottet C., Ricolleau C. (eds) Nanoalloys. Engineering Materials. Springer, London DOI:10.1007/ 978-1-4471-4014-6_3

[4] Lazzari, R. IsGISAXS: a program for grazing-incidence small-angle X-ray scattering analysis of supported islands. J. Appl. Crystallogr. 35, 406–421 (2002).

[5] Renaud, G., Lazzari, R., Leroy, F., Probing surface and interface morphology with Grazing Incidence Small Angle X-Ray Scattering. Surf. Sci. Rep. 64(8), 255-380 (2009).

[6] Penuelas, J., Andreazza, P., Andreazza-Vignolle, C., Tolentino, H.C.N., De Santis, M., Mottet, C., Controlling structure and morphology of CoPt nanoparticles through dynamical or static coalescence effects. Phys. Rev. Let. 100(11), 115502 (2008)

[7] Andreazza, P., Mottet, C., Andreazza-Vignolle, C., Penuelas, J., Tolentino, H.C.N., De Santis, M., Felici, R., Bouet, N., Probing nanoscale structural and order/disorder phase transitions of supported Co-Pt clusters under annealing. Physical Review B 82(15), 155453 (2010).

[8] Virot L., Andreazza P. (2006) XDSS Software, Orléans, France